



Structural, Magnetic and Catalytic Properties of FeCo Nanoparticles Synthesized by Polyol Process

Emre Can TAYFUN¹, Kaan ERMAN², Dogan KAYA^{3,4,*}, Faruk KARADAG⁵, Ahmet EKICIBIL⁶

¹*Cukurova University, Faculty of Art and Sciences, Department of Physics, Adana, Türkiye*
emrecontayfun@gmail.com, ORCID: 0009-0007-9343-7349

²*Imperial College London, Faculty of Natural Sciences, Department of Physics, London, United Kingdom*
kaanerman11@gmail.com, ORCID: 0009-0004-7541-8820

³*Cukurova University, Faculty of Art and Sciences, Department of Physics, Adana, Türkiye*

⁴*Cukurova University, Graduate School of Sciences, Department of Advance Materials and Nanotechnology, Adana, Türkiye*
dogankaya@cu.edu.tr, ORCID: 0000-0002-6313-7501

⁵*Cukurova University, Faculty of Art and Sciences, Department of Physics, Adana, Türkiye*
fkaradag@cu.edu.tr, ORCID: 0000-0001-7862-9085

⁶*Cukurova University, Faculty of Art and Sciences, Department of Physics, Adana, Türkiye*
ahmetcan@cu.edu.tr, ORCID: 0000-0003-3071-0444

Received: 07.08.2023

Accepted: 31.10.2023

Published: 31.12.2023

Abstract

Multi-functional FeCo nanoparticles (NPs) exhibit unique structural, magnetic, and catalytic properties, making them versatile materials with potential applications in diverse fields. In this work, we investigated the structural, electrochemical, and magnetic properties of as-prepared FeCo NPs synthesis by polyol method. X-ray diffraction analysis revealed multiphase structures: FeCo and α -Fe₂O₃ phases and scanning electron microscopy images confirmed spherical-like structures of FeCo NPs with an average size of 12.4 ± 0.1 nm. The electrochemical properties of FeCo NPs were investigated using a three-electrode setup in a 1 M KOH electrolyte at room temperature. The onset potentials for FeCo catalysts were found to be -0.15 V for ORR,



0.25 V for OER, and -1.26 V for HER. Tafel measurements further elucidated the reaction mechanism, revealing corrosion potentials of -0.165 V for ORR and 0.215 V for OER, with Tafel slopes of 228 mV dec⁻¹ and 48 mV dec⁻¹, respectively. A significant increase in magnetization was observed below 25 K in both zero-field-cooled and field-cooled curves, a magnetic transition temperature, T_s , occurs at 15 K, possibly indicating a ferromagnetic-to-antiferromagnetic phase transition. The hysteresis loop measurements revealed coercive field values ranging from 968 Oe at 5 K to approximately 206 Oe at 320 K, indicating a relaxation in magnetic spin orientation with increasing temperature. The saturation magnetization (M_s) values were recorded as 15.2 emu/g under a 5 T magnetic field, and the remanent magnetization (M_r) showed dominant ferromagnetic properties at 5 K with an M_r/M_s ratio indicating soft magnetic behavior. The magnetic susceptibility of FeCo NP exhibited a peak at approximately 25 K, and the Curie-Weiss law provided an estimated θ angle of -9.58°, suggesting antiferromagnetic interactions.

Keywords: FeCo NPs; Polyol; Structural; Magnetic; Catalytic.

Poliol Yöntemi ile Sentezlenen FeCo Nanopartiküllerinin Yapısal, Manyetik ve Katalitik Özellikleri

Öz

Çok işlevli FeCo nanoparçacıkları (NP'ler), manyetik, katalitik ve yapısal özelliklerin bir kombinasyonunu sergileyerek, çeşitli alanlarda potansiyel uygulamalara sahip çok yönlü malzemelerdir. Bu çalışmada, polioli yöntemi ile sentezlenen FeCo NP'lerin yapısal, elektrokimyasal ve manyetik özelliklerini araştırdık. X-ışını kırınım analizi, FeCo ve α -Fe₂O₃ fazlarını gösteren çoklu yapılar ortaya çıkardı ve taramalı elektron mikroskobu görüntüleri, ortalama boyutu 12.4 ± 0.1 nm olan küresel yapıları doğruladı. FeCo NP'lerin elektrokimyasal özellikleri, oda sıcaklığında 1 M KOH elektroliti içinde üç elektrot düzeneği kullanılarak incelendi. FeCo katalizörleri için başlangıç potansiyelleri, ORR (Oksijen indirgeme reaksiyonu) için -0.15 V, OER (Oksijen oluşum reaksiyonu) için 0.25 V ve HER (Hidrojen oluşum reaksiyonu) için -1.26 V olarak bulundu. Tafel ölçümleri, ORR için -0.165 V ve OER için 0.215 V'lik korozyon potansiyellerini ve sırasıyla 228 mV dec⁻¹ ve 48 mV dec⁻¹'lik Tafel eğimlerini ortaya çıkardı. Hem manyetik alanla soğutulmuş hem de manyetik alansız soğutulmuş eğrilerde 25 K'nin altında belirgin bir manyetizasyon artışı gözlemlendi ve 15 K'de bir manyetik bir geçiş sıcaklığı, T_s , gözlemlendi, bu da ferromanyetikten antiferromanyetik bir faz geçişini gösterebilir. Histeresis döngüsü ölçümleri, 5 K'de 968 Oe'den 320 K'de yaklaşık 206 Oe'ye kadar olan koersiv alan değerleri göstererek manyetik spin yönelmesinde bir gevşeme olduğunu gösterdi. 5 T manyetik alan altında doyum mıknatıslanması (M_s) değerleri 15.2 emu/g olarak kaydedildi ve 5

K'de kalıcı mıknatıslanma (M_r), domine ferromanyetik özellikleri gösterirken M_r/M_s oranı yumuşak manyetik davranışı gösterdi. Manyetik duyarlılık analizi, yaklaşık 25 K'de bir pik gösterdi ve Curie-Weiss yasası -9.58°K 'lik tahmini bir θ açısı sağlayarak antiferromanyetik etkileşimleri düşündürdü.

Anahtar Kelimeler: FeCo nanoparçacıklar; Poliöl; Yapısal; Manyetik; Katalitik.

1. Introduction

The development of advanced materials with tailored properties has become a key focus in scientific research, driven by the need for efficient and sustainable solutions to address contemporary challenges [1, 2]. In recent years, the synthesis and characterization of magnetic NPs have garnered significant attention due to their potential applications in various fields, including catalysis, biomedicine, and information storage [3, 4]. Iron-cobalt (FeCo) alloys have attracted significant attention due to their exceptional combination of magnetic and catalytic properties, rendering them promising candidates for a broad range of applications, including data storage, sensors, energy conversion, and catalysis [5-7]. FeCo NPs usually form an Fe-rich metallic core and a Co-rich surface layer composition [8] and this phenomenon can be attributed to the difference in the reduction potentials of Fe and Co [9]. FeCo NPs mostly used for oxygen evolution reaction (OER) and oxygen reduction reaction (ORR) activities. In a recent work by Park et al. [10] revealed that the overpotential for $\text{Fe}_{59}\text{Co}_{41}$ was significantly lower, measuring 285 mV at 10 mA cm^{-2} in a 1 M KOH solution, compared to the other samples. Furthermore, following chronopotentiometry at 10 mA cm^{-2} for 24 hours in 1 M KOH, the overpotential at 10 mA cm^{-2} increased slightly from 285 to 294 mV. The improved catalyst properties were attributed not only to the synergistic effect of the metal core and oxide layer but also to the beneficial influence of optimal iron doping.

Notably, there have been recent research efforts focused on studying FeCo soft magnetic nanomaterials [11, 12], which hold promise for diverse applications due to their exceptional magnetic characteristics, such as high saturation magnetization, large permeability, low coercivity, and ferromagnetic behavior up to 1073 K [13]. To fully exploit the potential of FeCo alloys, various synthesis methods have been explored, and the polyol process has emerged as a versatile and effective technique for the fabrication of FeCo NPs. The polyol process is a solution-based method that utilizes polyols, such as ethylene glycol, the solvent and reducing agent [14]. This approach offers several advantages, including precise control over the size, shape, and composition of nanoparticles, as well as a high degree of scalability. Moreover, the polyol process allows for the incorporation of stabilizers and dopants, further enhancing the properties and

functionalities of the resulting FeCo NPs [11]. In the literature, there are some studies reported for FeCo nanomaterials. For instance, FeCo prepared surfactant-assisted ball milling method with a size of 23 nm and saturation magnetization was recorded as $209 \text{ Am}^2 \cdot \text{kg}^{-1}$ (emu/g) [15]. Similarly, FeCo NPs synthesised using the polyol method and ethylene glycol (EG) as the solvent with a size of 30 nm and a saturation magnetization were recorded $200 \text{ Am}^2 \cdot \text{kg}^{-1}$ [11]. In other similar work, when the particle size is about 8 μm , the saturation magnetization was found to be $220 \text{ Am}^2 \cdot \text{kg}^{-1}$ [16].

In this paper, we aim to provide the structural, magnetic, and catalytic properties of FeCo NP prepared using the polyol process. Structural analysis provided multiphase structure FeCo formation with narrow particle size distribution. With this structural formation, FeCo catalyst exhibited promising results for ORR and OER activities. Moreover, a detailed investigation of magnetic properties using *M-T* and *M-H* curves revealed a large coercive field and relatively low saturation magnetization.

2. Materials and Methods

2.1. Chemicals

Iron(III) acetylacetonate ($\text{Fe}(\text{acac})_3$, $\geq 97\%$), cobalt acetylacetonate ($\text{Co}(\text{acac})_2$, $\geq 99.0\%$) metal salts, polyvinylpyrrolidone (PVP, average mol wt. 40000) surfactant, N, N-dimethylformamide (DMF $\geq 99.0\%$), ethylene glycol (EG $\geq 99.0\%$), sodium hydroxide (NaOH $\geq 99.0\%$), dichloromethane ($\geq 99.0\%$), ethanol absolute ($\geq 99.9\%$), and sodium borohydride (NaBH_4 $\geq 98.0\%$) were purchased from Sigma Aldrich. All chemicals were used as received without further purification.

2.2. Synthesis of FeCo NPs

The synthesis process and chemicals used for FeCo NPs are presented in Figure 1. 1.7 mmol Fe and 1.7 mmol Co metal salts were dissolved in 25 ml of DMF. The resulting mixture was then poured into a three-necked round-bottom flask containing 60 ml EG (with an EG/FeCo mole ratio of 300), serving as a low-temperature reducing agent. The solution mixed with PVP to prevent agglomeration (with an EG/FeCo mole ratio of 4), and NaOH (with an EG/FeCo mole ratio of 15) to stabilize pH (orange like color). The reaction was carried out at 30 °C under a constant flow of Ar gas and vigorous magnetic stirring. Subsequently, the mixture temperature was raised to 130 °C, and the secondary reducing agent NaBH_4 (with an EG/FeCo mole ratio of 24), previously dissolved in 25 ml DMF, was slowly added dropwise into the mixture over 5 minutes (brown-black color). The solution was then refluxed at 150 °C for 60 minutes, during

which the black color indicated the successful reduction of the FeCo NPs. Afterward, the solution was cooled down to room temperature, washed with ethanol to remove most of the by-products, and subjected to sanctification cycles at 9000 rpm. Finally, the resulting product was dried at 55 °C for 24 hours.

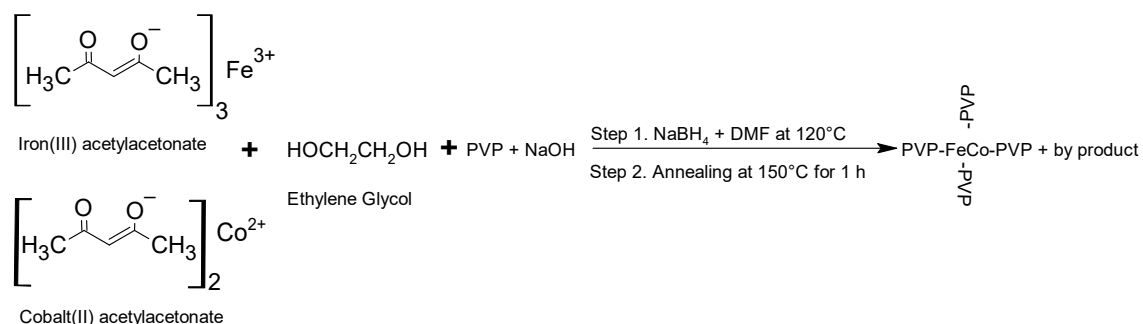


Figure 1: Chemical process of the synthesis of PVP decorated FeCo NPs

2.3. Characterizations of FeCo NPs

X-ray diffraction (XRD, using $\text{Cu-K}\alpha$ radiation ($\lambda=1.54 \text{ \AA}$)), was obtained for the structural analysis of the samples, and subsequently, Scanning electron microscopy (SEM) and energy-dispersive x-ray spectroscopy (EDS) data were collected to determine the morphology, the average size distribution and the chemical composition of FeCo NPs through stoichiometric calculations, respectively. The magnetic properties of FeCo NPs were investigated using a physical property measurement system with a vibrating sample magnetometer, as a function of temperature in a range of 5–380 K and applied field of $\pm 5 \text{ T}$ at 5 K, 100 K, 300 K and 320 K.

2.4. Electrochemical measurements of FeCo NPs

The Gamry 1010E potentiostat was utilized for all electrochemical measurements. The system featured a conventional three-electrode setup, comprising a reference electrode with a 3 M KCl-saturated Ag/AgCl, a counter electrode with a $6 \times 6 \text{ mm}^2$ platinum (99.95% pure) and a working electrode with a carbon rod of 5 mm diameter. To prepare the working electrode, 1 mg of FeCo NPs was mixed with $7 \mu\text{l}$ EG, $5 \mu\text{l}$ DMF, and $2 \mu\text{l}$ of 5% Nafion. The mixture was sonicated for 15 minutes and then vortexed for 2 minutes. Following, this ink was dropped onto a carbon electrode and dried in a furnace for 16 hours. Cyclic voltammetry (CV) measurements were performed in a 1 M KOH alkaline solution with a scan rate of 5, 25, 50, 75, and 100 mV s^{-1} and a step size of 2 mV, within the potential range between -1.2 and 1.2 V vs. Ag/AgCl. Additionally, linear sweep

voltammetry (LSV) measurements were carried out to investigate the ORR, OER and hydrogen evolution reaction (HER) activities, with a fixed scan rate of 50 mV s⁻¹.

3. Results and Discussion

3.1. Characterization of FeCo NPs

The structural properties of the as-prepared FeCo NPs were determined using XRD. Figure 2(a) displays the experimental XRD data of FeCo NPs (black line), which was measured for 2θ ranging from 20° to 100° using Cu- $K\alpha$ radiation. The XRD analysis revealed a multiphase structure for the NPs, with peaks at $2\theta=35.6^\circ$, 59° corresponding to the FeCo phase (CoFe₂O₄) [17] and a peak at $2\theta=33.8^\circ$ assigned to the α -Fe₂O₃ phase [18]. This indicates that FeCo NPs were partially oxidized, forming the α -Fe₂O₃ phase in the structure [17]. In Figure 2(b), EDS data for FeCo NPs with elemental analysis for Fe, Co, O and C elements and their energy shells are illustrated [5]. The stoichiometry of Fe and Co elements was calculated by collecting EDS data from five different areas, as shown in the inset table of Figure 2(b) [19]. The counts of oxygen atoms were highest compared to Fe and Co due to oxide phases in the structure, as revealed by the XRD profile, and the C signal originated from the carbon tape sample holder. The stoichiometry analysis showed the K and L shells of Fe and Co, respectively. The entry ratio of Fe and Co precursors aimed for Fe_{0.50}Co_{0.50}, and the obtained stoichiometry was Fe_{0.49}Co_{0.51}, which was quite similar to the entry ratio [20]. Additional peaks observed at 1.04 keV and 2.121-9.67 keV belonged to sodium (Na) [21] and gold (Au) elements [22], respectively. These peaks originated from residue chemicals in the structure, where NaBH₄ was used as a secondary reducing agent, and NaOH served as a pH stabilizer to reduce the particle size. The presence of Au peaks was due to the Au-covered surface to improve SEM resolution before the imaging process. In Figure 2(c), SEM images of the FeCo NPs are presented. The average size distribution of FeCo NPs is shown in Figure 2(d), where approximately 250 particles were counted by analyzing several SEM images at a magnification of 600000X. The observed spherical-like structures in SEM images were due to the presence of PVP molecules. The size distribution of FeCo NPs ranged from 8 to 18 nm, as seen in Figure 2(d). To determine the average size of the NPs, a log-normal fit function was applied, yielding an average size of 12.4 ± 0.1 nm.

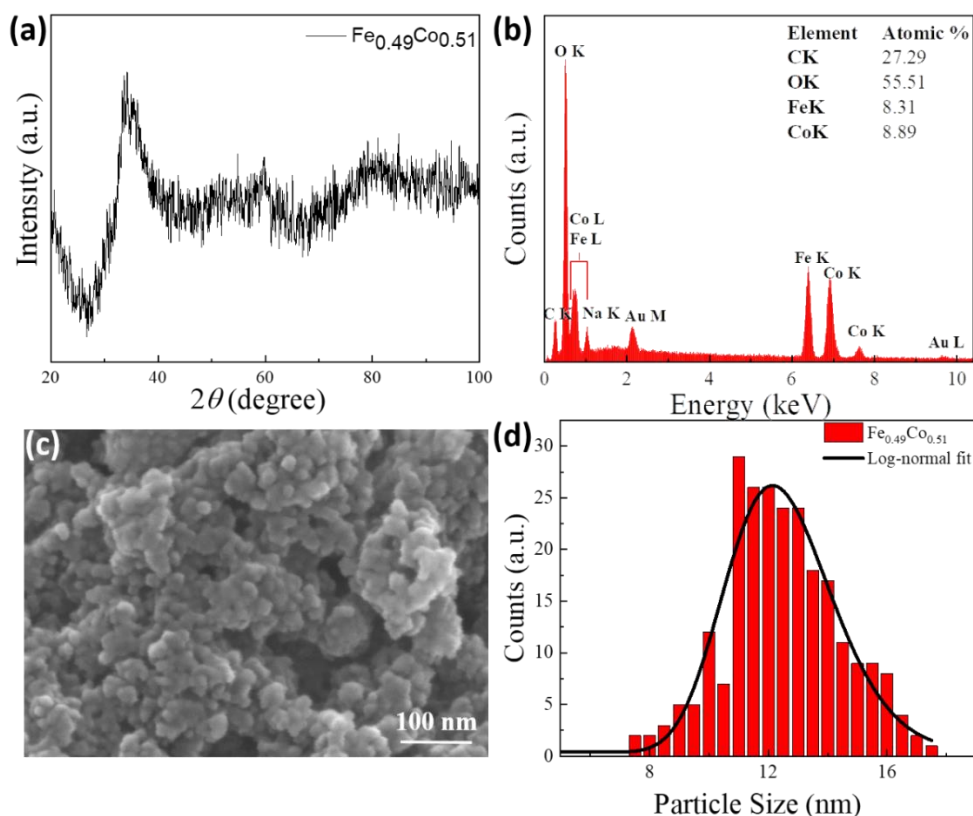


Figure 2: (a) XRD profile of FeCo NPs, (b) EDS data showing elemental analysis for Fe, Co, O and C, (c) SEM image, (d) The average particle size (red bar) dispersion fitted by a log-normal dispersion (dark black line) for sample

3.2. Electrochemical Properties of FeCo NPs

The electrochemical properties of FeCo NPs were investigated using a three-electrode setup in 1 M KOH at room temperature. Initially, the CV curves of FeCo NPs were recorded in the voltage range of -1.2 V to +1 V (vs. Ag/AgCl) to elucidate the adsorption/desorption mechanism of O and H atoms, as well as the reduction/evolution steps. Figure 3(a) illustrates the CV results, indicating weak H₂ gas desorption below -1.2 V and clear O₂ gas evolution after OH adsorption/O formation around 0.4 V. Additionally, FeCo NPs exhibited an enhanced oxygen reduction peak around -0.5 V. Furthermore, CV measurements were conducted at various scan rates of 5 mV s⁻¹ (grey line), 25 mV s⁻¹ (red line), 50 mV s⁻¹ (blue line), 75 mV s⁻¹ (green line), and 100 mV s⁻¹ (purple line), as shown in Figure 3(b). With an increase in scan rate from 5 mV s⁻¹ to 100 mV s⁻¹, the anodic peak potential shifted slightly towards a more positive potential. The measurements were normalized for comparison, and the results indicated that as the scan rate increased, the current response to potential also increased, confirming the faradaic behavior of the FeCo electrode [23].

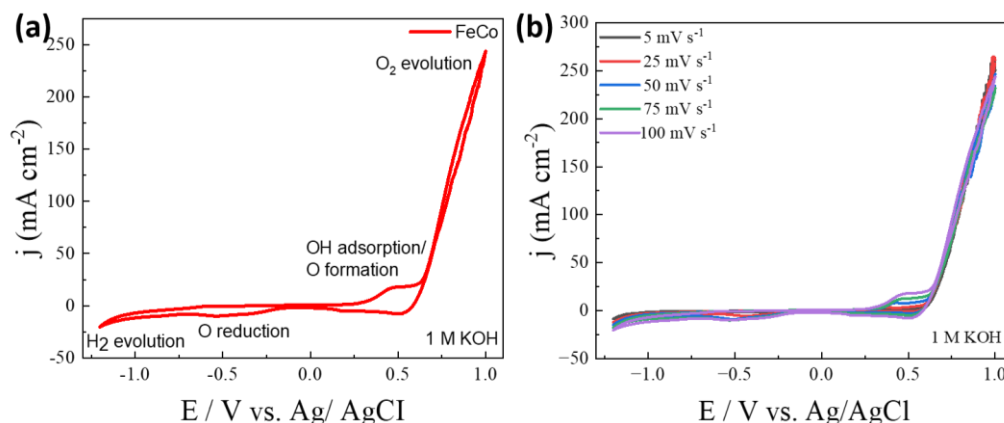


Figure 3: (a) CV curves of $\text{Fe}_{0.49}\text{Co}_{0.51}$ (red line), alloys in 1 M KOH at room temperature with a scan rate of 100 mV s^{-1} , (b) CV graph at different scan rates are 5 mV s^{-1} (grey line), 25 mV s^{-1} (red line), 50 mV s^{-1} (blue line), 75 mV s^{-1} (green line), and 100 mV s^{-1} (purple line), respectively

Further, detailed investigation of FeCo NPs was conducted through ORR (orange line), OER (green line), and HER (blue line) polarization curves at a scan rate of 50 mV s^{-1} in 1 M KOH (see Figure 4(a, b and c), respectively). The onset potentials for FeCo catalysts were determined to be -0.15 V for ORR, 0.25 V for OER and -1.26 V for HER, respectively. Remarkably, FeCo catalyst exhibited a promising potential for ORR, surpassing commercially available Pt/C with an onset potential of -0.05 V [24]. Notably, the current density of FeCo catalyst recorded above 10 mA cm^{-2} for ORR, which is twice as high as the commercial Pt/C catalyst at 5 mA cm^{-2} in 1 M KOH. In terms of OER, FeCo catalyst demonstrated superior performance with a 0.25 V improvement compared to commercially available IrO_2 and RuO_2 catalysts with 0.3 V [25, 26]. The overpotentials at 50 mA cm^{-2} and 100 mA cm^{-2} were found to be 0.48 V and 0.71 V , respectively. However, it is evident that the catalysis activity of FeCo for HER exhibited a high onset potential due to the oxide formation in the FeCo structure. To further elucidate the reaction mechanism, Tafel measurements were conducted in 1 M KOH at room temperature for ORR (red line) and OER (black line) processes (see Figure 4(d)). The corrosion potentials were recorded -0.165 V and 0.215 V for ORR and OER, respectively. The corrosion potentials were recorded as -0.165 V and 0.215 V and with Tafel slopes of 228 mV dec^{-1} and 48 mV dec^{-1} for ORR and OER, respectively.

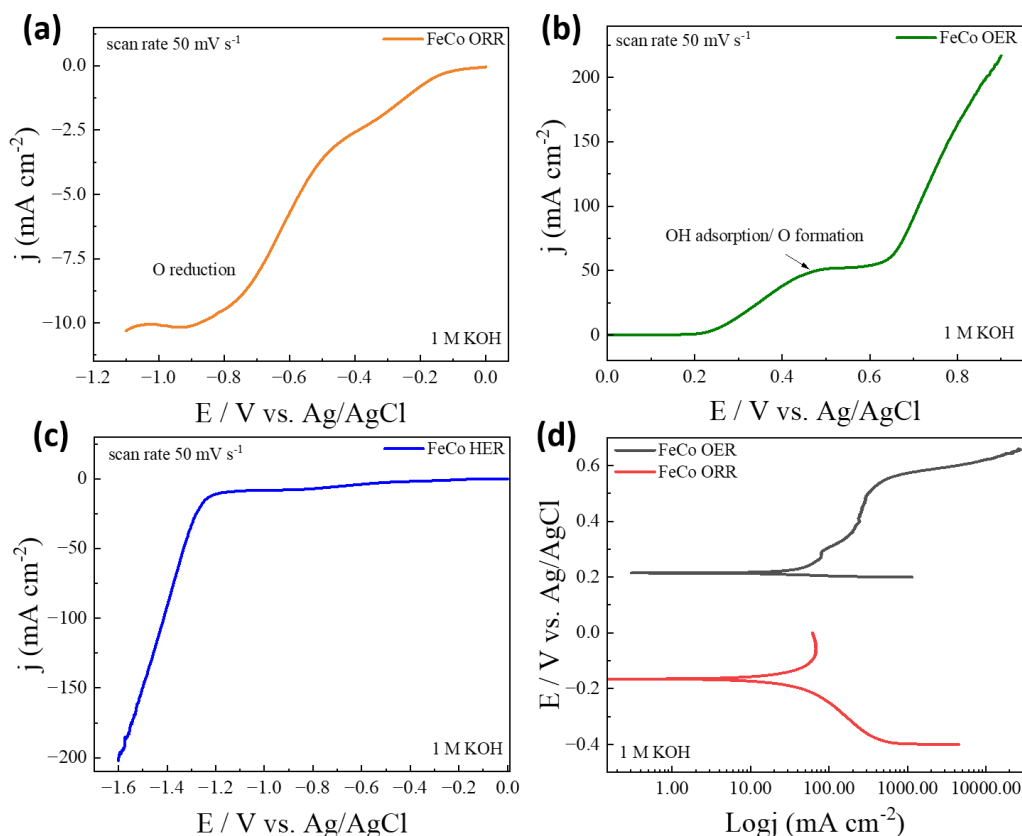


Figure 4: (a-c) The LSV curves shown in 50 mVs^{-1} in 1 M KOH are ORR (orange line), OER (green line), HER (blue line), respectively, (d) Tafel OER (black line) and OER (red line) curves

3.2. Magnetic Properties of FeCo NPs

Figure 5(a) depicts the magnetic moment as a function of temperature (M - T) in the range of 5-380 K for ZFC (hollow circle) and FC (solid circle) curves with an applied field of 500 Oe. The magnetization of FeCo NPs increased as the temperature decreased from 380 K to 5 K, and a significant increase was observed below 25 K in the FC curve. Similarly, the ZFC curve also showed an increase with decreasing temperature between 380 K and 31 K, which is referred to as the blocking temperature, T_B . At this point, thermal energy decreases, leading to a net alignment of spins in the ferromagnetic FeCo NPs. This alignment is attributed to the presence of small particles in the sample [6]. Subsequently, the magnetization decreased, and a sudden increase was observed below 15 K, indicating a magnetic phase transition, at a temperature of T_s . This magnetic phase transition at below 15 K force the spins alignment to applied magnetic field which results in ferromagnetic contribution so that magnetization increases with decreasing temperature. There is a reduction in ZFC magnetization below T_B which is the presence of an antiferromagnetic signal in the sample surface may arise from the α - Fe_2O_3 phase. The magnetization behavior of Fe-oxide varies with particle size, influenced by the surface spin effect, which leads to decreased

magnetization for smaller nanoparticles [27]. Additionally, changes in particle size or fluctuations in temperature can also control this behavior.

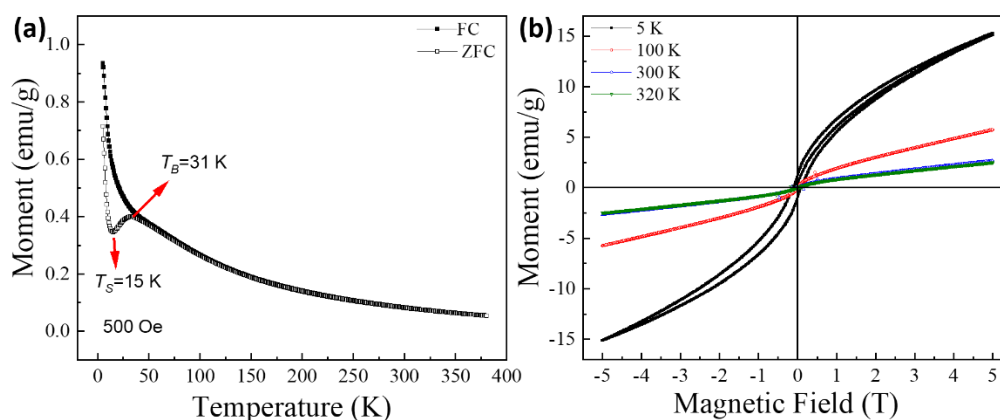


Figure 5: (a) M - T plot in range of 5-380 K for ZFC (hollow circle) and FC (solid circle) curves showing temperature transitions at $T_B=31$ K and $T_S=15$ K under magnetic field of 500 Oe, (b) M - H plot recorded at 5 K (black), 100 K (red), 300 K (blue) and 320 K (green) between ± 5 T

Figure 5(b) illustrates the hysteresis loop measurements as a function of temperature for the $\text{Fe}_{0.49}\text{Co}_{0.51}$ sample. The magnetic behavior was investigated at temperatures of 5 K (black line), 100 K (red line), 300 K (blue line), and 320 K (green line). Clear hysteresis loop gaps were observed, indicating the presence of a coercive field (H_c) at all temperatures. The H_c values were found to be 968 Oe at 5 K, gradually decreasing to approximately 206 Oe with increasing temperature, which suggests a relaxation in magnetic spin orientation [6, 28]. Additionally, while a dominant ferromagnetic effect was observed below $T_S=15$ K, an antiferromagnetic contribution was observed as the temperature increased, providing an explanation for the behavior of H_c [29]. The substantial coercivity measuring 968 Oe, which is notably higher than the typically low coercivities observed in soft magnetic FeCo, serves as evidence indicating that the particles do not exhibit superparamagnetic behavior [30].

The saturation magnetization (M_s) value was recorded as approximately 15.2 emu/g under a 5 T magnetic field. The decrease in M_s relative to the bulk is ascribed to the existence of a thin oxide layer of the $\alpha\text{-Fe}_2\text{O}_3$ phase on the surface of the particles, which forms rapidly upon exposure to air. However, the hysteresis curve indicated that the sample did not reach full-saturation magnetization at 5 K. This suggests that the magnetic field strength and magnetization increase at the same rate as the temperature applied to the material increases. Similar results were obtained for $\text{Fe}_{0.49}\text{Co}_{0.51}$ NPs, with a maximum M_s of 60 emu/g, attributed to oxidation-free synthesis and small particle size in the range of 1.34 to 2.47 nm [13, 31]. Consequently, as the temperature approaches 5 K, entropy decreases, thermal degradation does not occur, and the

material exhibits regularity, leading to an increase in the magnetic moment of the material and thereby increasing the magnetization [32, 33].

Moreover, the remanent magnetization (M_r) of the material was determined as 1.08 emu/g at 5 K and 0.03 emu/g at 300 K and 320 K, yielding approximately the same value. Therefore, the result of about 1.08 emu/g at 5 K indicates that the material exhibits dominant ferromagnetic properties at 5 K, which can be attributed to oxidation. The M_r/M_s ratio was calculated to provide information about the magnetic characterization of the material, indicating that the resulting compound possesses soft magnetic properties. The M_p values shifted positively at 5 and 100 K, but negatively at 300 and 320 K. Detailed magnetization results of the sample are recorded in Table 1.

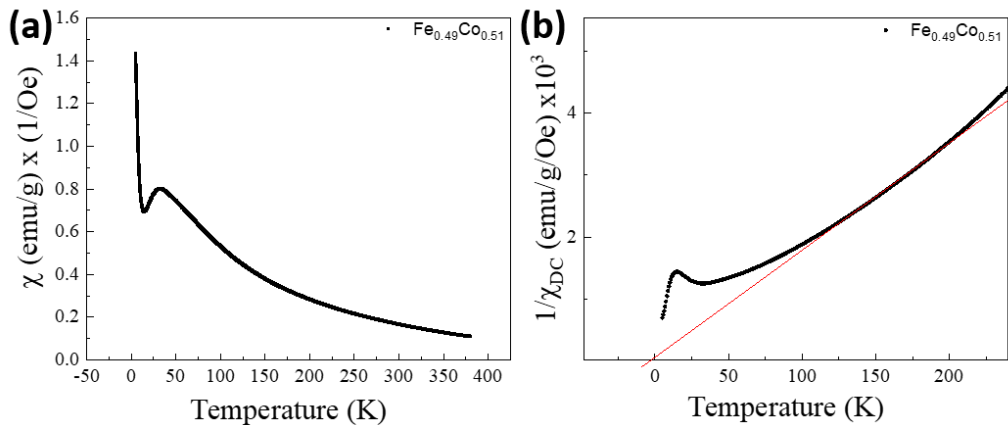


Figure 6: (a) χ - T graph, and (b) $1/\chi$ - T and with linear fit

Magnetic susceptibility measurements for FeCo NPs are presented in Figure 6(a and b), which depicts the χ and $1/\chi_{DC}$ graphs with a linear fit (red line) applied to these curves. The data were calculated using the Curie-Weiss law with the aid of a linear fit for $1/\chi_{DC} = (T - \theta)/C$. In Figure 6(a), the magnetic susceptibility decreases from 380 K, reaches a peak at approximately 25 K, and then decreases to 0 K. Consequently, the value of the θ angle was determined as -9.58° based on the linear slope of this graph. Furthermore, upon further examination of Figure 6(b), it is observed that the magnetic susceptibility experiences a decrease of 0.7 Oe^{-1} , followed by another peak, indicating an initial increase and then a subsequent decrease, ultimately converging to a descending curve toward 380 K [34].

Table 1: Measured values of the magnetic properties of FeCo

$\text{Fe}_{0.49}\text{Co}_{0.51}$	H_c (Oe)	H_e (Oe)	M_s (emu/g)	M_r (emu/g)	M_p (emu/g)	M_r/M_s
5 K	968.4	94.3	15.20	1.08	0.136	0.071
100 K	214.5	8.5	5.74	0.12	0.001	0.021
300 K	192.5	13.5	2.64	0.03	-0.001	0.012
320 K	206.5	11.5	2.49	0.03	-0.001	0.012

4. Conclusion

In conclusion, the multi-functional FeCo nanoparticles (NPs) synthesized through the polyol method display a diverse range of magnetic, catalytic, and structural properties, making them highly versatile materials with significant potential for various applications. The investigation of their structural, electrochemical, and magnetic characteristics revealed multiphase structures consisting of FeCo and α -Fe₂O₃ phases. The spherical-like structures of FeCo NPs, with an average size of 12.4 ± 0.1 nm, were confirmed through scanning electron microscopy. The electrochemical studies demonstrated promising catalytic activities of FeCo NPs for oxygen reduction reaction (ORR), oxygen evolution reaction (OER), and hydrogen evolution reaction (HER), with onset potentials of -0.15 V, 0.25 V, and -1.26 V, respectively. Tafel measurements provided further insights into the reaction mechanism, unveiling corrosion potentials of -0.165 V for ORR and 0.215 V for OER, along with respective Tafel slopes. Additionally, magnetization studies exhibited intriguing behavior below 25 K, indicating a magnetic transition at $T_s=15$ K, possibly implying a ferromagnetic-to-antiferromagnetic phase transition. The hysteresis loop measurements revealed temperature-dependent H_c values, indicative of magnetic spin orientation relaxation. Furthermore, the M_s values recorded at 5 T magnetic field and the M_r at 5 K highlighted the dominant ferromagnetic properties of the FeCo NPs, suggesting soft magnetic behavior. The magnetic susceptibility analysis further supported the presence of antiferromagnetic interactions with a peak at approximately 25 K. Overall, these findings contribute valuable insights into the multi-faceted properties of FeCo NPs and their potential for a wide range of applications in various fields.

Acknowledgements

This work was primarily supported by Cukurova University, Adana, Turkey, under Scientific Research Funding Grand No: FBA-2021-13479.

References

- [1] Zhang, H.-M., Wang, J.-J., Meng, Y., Sun, J., *Recent advances in amorphous metal phosphide electrocatalysts for hydrogen evolution reaction*, International Journal of Hydrogen Energy, 47(85), 36084-36097, 2022.
- [2] Kim, J.S., Kim, B., Kim, H., Kang, K., *Recent progress on multimetal oxide catalysts for the oxygen evolution reaction*, 8(11), 1702774, 2018.
- [3] Litvinov, D., Chunseng, E., Parekh, V., Smith, D., Rantschler, J., Zhang, S., Donner, W., Lee, T.R., Ruchhoeft, P., Weller, D., Khizroev, S., *Design and fabrication of high anisotropy nanoscale bit-patterned magnetic recording medium for data storage applications*, ECS Transactions, 3(25), 249-258, 2019.

[4] Liu, Y., Li, D., Sun, S., *Pt-Based composite nanoparticles for magnetic, catalytic, and biomedical applications*, *Journal of Materials Chemistry*, 21(34), 12579-12587, 2011.

[5] Koutsopoulos, S., Barfod, R., Eriksen, K.M., Fehrmann, R., *Synthesis and characterization of iron-cobalt (FeCo) alloy nanoparticles supported on carbon*, *Journal of Alloys and Compounds*, 725, 1210-1216, 2017.

[6] Shokuhfar, A., Afghahi, S.S.S., *Size controlled synthesis of FeCo alloy nanoparticles and study of the particle size and distribution effects on magnetic properties*, *Advances in Materials Science and Engineering*, 2014, 1-10, 2014.

[7] Liu, X.G., Geng, D.Y., Ma, S., Meng, H., Tong, M., Kang, D.J., Zhang, Z.D., *Electromagnetic-wave absorption properties of FeCo nanocapsules and coral-like aggregates self-assembled by the nanocapsules*, *Journal of Applied Physics*, 104(6), 064319, 2008.

[8] Park, J.-H., Woo, S., Lee, J., Jung, H.Y., Ro, J.C., Park, C., Lim, B., Suh, S.-J., *Facile modified polyol synthesis of FeCo nanoparticles with oxyhydroxide surface layer as efficient oxygen evolution reaction electrocatalysts*, *International Journal of Hydrogen Energy*, 46(29), 15398-15409, 2021.

[9] Larcher, D., Patrice, R., *Preparation of metallic powders and alloys in polyol media: a thermodynamic approach*, *Journal of Solid State Chemistry*, 154(2), 405-411, 2000.

[10] Park, J.-H., Ro, J.C., Suh, S.-J., *FeCo nanoparticles with different compositions as electrocatalysts for oxygen evolution reaction in alkaline solution*, *Applied Surface Science*, 589, 153041, 2022.

[11] Zamanpour, M., Chen, Y., Hu, B., Carroll, K., Huba, Z.J., Carpenter, E.E., Lewis, L.H., Harris, V.G., *Large-scale synthesis of high moment feco nanoparticles using modified polyol synthesis*, *Journal of Applied Physics*, 111(7), 2012.

[12] Rafique, M.Y., Pan, L., Zubair Iqbal, M., Javed, Q.-u.-a., Qiu, H., Rafi ud, d., Farooq, M.H., Guo, Z., *3-D flower like FeCo alloy nanostructures assembled with nanotriangular prism: facile synthesis, magnetic properties, and effect of NaOH on its formation*, *Journal of Alloys and Compounds*, 550, 423-430, 2013.

[13] Yang, F.J., Yao, J., Min, J.J., Li, J.H., Chen, X.Q., *Synthesis of high saturation magnetization FeCo nanoparticles by polyol reduction method*, *Chemical Physics Letters*, 648, 143-146, 2016.

[14] Fiévet, F., Ammar-Merah, S., Brayner, R., Chau, F., Giraud, M., Mammeri, F., Peron, J., Piquemal, J.Y., Sicard, L., Viau, G., *The polyol process: a unique method for easy access to metal nanoparticles with tailored sizes, Shapes And Compositions*, *Chemical Society Reviews*, 47(14), 5187-5233, 2018.

[15] Poudyal, N., Rong, C.-b., Liu, J.P., *Morphological and magnetic characterization of Fe, Co, and FeCo nanoplates and nanoparticles prepared by surfactants-assisted ball milling*, *Journal of Applied Physics*, 109, 07B526, 2011.

[16] Hiyama, H., Kodama, D., Matsumoto, T., Shinoda, K., Kasuya, R., Balachandran, J., *Synthesis and magnetic properties of platelet Fe-Co particles*, *Journal of Applied Physics*, 107(9), 2010.

- [17] Zehani, K., Bez, R., Moscovici, J., Mazaleyrat, F., Mliki, N., Bessais, L., *High magnetic moment of FeCo nanoparticles produced in polyol medium*, IEEE Transactions on Magnetics, 50(4), 1-5, 2014.
- [18] Suman, S., Chahal, S., Kumar, A., Kumar, P., *Zn Doped α -Fe₂O₃: An efficient material for UV driven photocatalysis and electrical conductivity*, 10(4), 273, 2020.
- [19] Farahmandjou, M., Honarbakhsh, S., Behrouzina, S., *FeCo nanorods preparation using new chemical synthesis*, Journal of Superconductivity and Novel Magnetism, 31(12), 4147-4152, 2018.
- [20] Hossain, M.A., *Synthesis of carbon nanoparticles from kerosene and their characterization by SEM/EDX, XRD and FTIR*, American Journal of Nanoscience and Nanotechnology, 1(2), 2013.
- [21] Zhang, M., Lin, Y., Mullen, T.J., Lin, W.-f., Sun, L.-D., Yan, C.-H., Patten, T.E., Wang, D., Liu, G.-y., *Improving Hematite's solar water splitting efficiency by incorporating Rare-Earth upconversion nanomaterials*, The Journal of Physical Chemistry Letters, 3(21), 3188-3192, 2012.
- [22] Cappellari, P.S., Baena-Moncada, A.M., Coneo-Rodríguez, R., Moreno, M.S., Barbero, C.A., Planes, G.A., *Catalytic enhancement of formic acid electro-oxidation through surface modifications with gold on supported Pt nanoparticles*, International Journal of Hydrogen Energy, 44(3), 1967-1972, 2019.
- [23] Puratchi Mani, M., Ponnarasi, K., Rajendran, A., Venkatachalam, V., Thamizharasan, K., Jothibas, M., *Electrochemical behavior of an advanced FeCo₂O₄ electrode for supercapacitor applications*, Journal of Electronic Materials, 49(10), 5964-5969, 2020.
- [24] Gao, F., Zhang, Y., Wu, Z., You, H., Du, Y., *Universal strategies to multi-dimensional noble-metal-based catalysts for electrocatalysis*, Coordination Chemistry Reviews, 436, 213825, 2021.
- [25] Meierhofer, F., Fritsching, U., *Synthesis of metal oxide nanoparticles in flame sprays: review on process technology, modeling, and diagnostics*, Energy & Fuels, 35(7), 5495-5537, 2021.
- [26] Yoo, H., Oh, K., Lee, Y.R., Row, K.H., Lee, G., Choi, J., *Simultaneous co-doping of RuO₂ And IrO₂ into Anodic TiO₂ Nanotubes: A binary catalyst for electrochemical water splitting*, International Journal of Hydrogen Energy, 42(10), 6657-6664, 2017.
- [27] Sun, S., Zeng, H., Robinson, D.B., Raoux, S., Rice, P.M., Wang, S.X., Li, G., *Monodisperse MFe₂O₄ (M = Fe, Co, Mn) nanoparticles*, Journal of the American Chemical Society, 126(1), 273-279, 2004.
- [28] Wesselinowa, J.M., Apostolova, I., *Size, Anisotropy and doping effects on the coercive field of ferromagnetic nanoparticles*, Journal of Physics: Condensed Matter, 19(40), 406235, 2007.
- [29] Sort, J., Nogués, J., Amils, X., Suriñach, S., Muñoz, J.S., Baró, M.D., *Room-temperature coercivity enhancement in mechanically alloyed antiferromagnetic-ferromagnetic powders*, Applied Physics Letters, 75(20), 3177-3179, 1999.

[30] Karipoth, P., Thirumurugan, A., Velaga, S., Greneche, J.-M., Justin Joseyphus, R., *Magnetic properties of FeCo alloy nanoparticles synthesized through instant chemical reduction*, Journal of Applied Physics, 120(12), 2016.

[31] Kemp, S.J., Ferguson, R.M., Khandhar, A.P., Krishnan, K.M., *Monodisperse magnetite nanoparticles with nearly ideal saturation magnetization*, RSC Advances, 6(81), 77452-77464, 2016.

[32] Kurniawan, M., Perrin, A., Xu, P., Keylin, V., McHenry, M., *Curie temperature engineering in high entropy alloys for magnetocaloric applications*, IEEE Magnetics Letters, 7, 1-5, 2016.

[33] Goya, G.F., Berquó, T.S., Fonseca, F.C., Morales, M.P., *Static and dynamic magnetic properties of spherical magnetite nanoparticles*, Journal of Applied Physics, 94(5), 3520-3528, 2003.

[34] Stipe, B.C., Rezaei, M.A., Ho, W., Gao, S., Persson, M., Lundqvist, B.I., *Single-molecule dissociation by tunneling electrons*, Physical Review Letters, 78(23), 4410-4413, 1997.